

PROGRESS IN NANOTECHNOLOGY

Processing

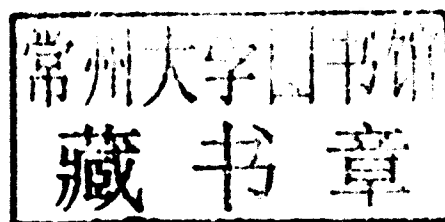
**The
American
Ceramic
Society**



Progress in Nanotechnology

Processing

A Progress in Ceramic Technology series publication



 **WILEY**

A John Wiley & Sons, Inc., Publication

Copyright © 2010 by The American Ceramic Society. All rights reserved.

Published by John Wiley & Sons, Inc., Hoboken, New Jersey.
Published simultaneously in Canada.

No part of this publication may be reproduced, stored in a retrieval system, or transmitted in any form or by any means, electronic, mechanical, photocopying, recording, scanning, or otherwise, except as permitted under Section 107 or 108 of the 1976 United States Copyright Act, without either the prior written permission of the Publisher, or authorization through payment of the appropriate per-copy fee to the Copyright Clearance Center, Inc., 222 Rosewood Drive, Danvers, MA 01923, (978) 750-8400, fax (978) 750-4470, or on the web at www.copyright.com. Requests to the Publisher for permission should be addressed to the Permissions Department, John Wiley & Sons, Inc., 111 River Street, Hoboken, NJ 07030, (201) 748-6011, fax (201) 748-6008, or online at <http://www.wiley.com/go/permission>.

Limit of Liability/Disclaimer of Warranty: While the publisher and author have used their best efforts in preparing this book, they make no representations or warranties with respect to the accuracy or completeness of the contents of this book and specifically disclaim any implied warranties of merchantability or fitness for a particular purpose. No warranty may be created or extended by sales representatives or written sales materials. The advice and strategies contained herein may not be suitable for your situation. You should consult with a professional where appropriate. Neither the publisher nor author shall be liable for any loss of profit or any other commercial damages, including but not limited to special, incidental, consequential, or other damages.

For general information on our other products and services or for technical support, please contact our Customer Care Department within the United States at (800) 762-2974, outside the United States at (317) 572-3993 or fax (317) 572-4002.

Wiley also publishes its books in a variety of electronic formats. Some content that appears in print may not be available in electronic format. For information about Wiley products, visit our web site at www.wiley.com.

Library of Congress Cataloging-in-Publication Data:

Progress in nanotechnology : processing.

p. cm. — (Progress in ceramic technology)

Includes index.

ISBN 978-0-470-40839-1 (cloth)

1. Nanostructured materials. 2. Nanotechnology.

TA418.9.N35P765 2010

620'.5—dc22

2009035822

Printed in the United States of America.

10 9 8 7 6 5 4 3 2 1

Progress in Nanotechnology

Introduction

Although nanotechnology is still an emerging industry, it represents a huge potential in a variety of markets that include biomedical, electronics, and energy totaling billions of dollars. However, before these markets are realized, processing methods must be developed that can produce quality nanomaterials and structures. Whether the material is a powder, thin film, wire, or composite, an optimal processing method is needed.

Powders of various compositions can be made by a wide range of methods, including freeze casting, chemical, hydrothermal synthesis, and solution combustion, among others. Each method has its limitations and advantages. The methods to make thin films and coatings include chemical vapor deposition, spray pyrolysis, and sol gel. Wires can be made by electrospinning or hydrothermal synthesis. Other methods are under development for making composites and other structures.

This edition of *Progress in Ceramic Technology* series contains a select compilation of articles on the topic of nanomaterials processing of powders; thin films, wires and tubes; and composites that were previously published in *The American Ceramic Society Bulletin*, *Journal of the American Ceramic Society*, *International Journal of Applied Ceramic Technology*, *Ceramic Engineering and Science Proceedings* (CESP) and *Ceramic Transactions* (CT).

The American Ceramic Society contributes to the progress of nanotechnology by providing forums for information exchange during its various meetings and by publishing articles in its various journals and proceedings.

For other books on nanotechnology, including *Progress in Nanotechnology: Applications*, visit the ACerS bookstore at www.ceramics.org or the ACerS-Wiley webpage at www.wiley.com/go/ceramics.

Contents

Introduction	xi
Synthesis Methods for Powders	
Freeze Casting as a Nanoparticle Material-Forming Method K. Lu and X. Zhu <i>Int. J. of Appl. Ceram. Technol.</i> , Vol. 5, Is. 3, p. 219-227	3
Preparation of a Nanoscale/SOFC-Grade Yttria-Stabilized Zirconia Material: A Quasi-Optimization of the Hydrothermal Coprecipitation Process Y-C Chang, M-C Lee, W-X Kao, and T-N Lin <i>Int. J. of Appl. Ceram. Technol.</i> , Vol. 5, Is. 6, p. 557-567	13
Synthesis of Nanosize Tin Dioxide by a Novel Liquid-Phase Process Y. Zhou, N. Dasgupta, and A. Virkar <i>J. Am. Ceram. Soc.</i> , Vol. 91, No. 3, p. 1009-1012, 2008	25
Fabrication of Nanocomposite Powders of Carbon Nanotubes and Montmorillonite J. Feng and Q. Wang <i>J. Am. Ceram. Soc.</i> , Vol. 91, No. 3, p. 975-978, 2008	29
Synthesis of Highly Dispersed Barium Titanate Nanoparticles by a Novel Solvothermal Method X. Wei, G. Xu, Z. Ren, Y. Wang, G. Shen, and G. Han <i>J. Am. Ceram. Soc.</i> , Vol. 91, No. 1, p. 315-318, 2008	33
Continuous Production and Harvesting of Inorganic-Ceramic Nanoparticles S.A.E. Abdulla, P.A. Sermon, M. Worsley, and I.R. Collins <i>CESP</i> , Vol. 28, No. 6, p. 131-141, 2008	37
Nanocrystalline Scandia Powders Via Oxalate Precipitation: The Effects of Solvent and Solution pH Z. Xiu, J-G. Li, X. Li, D. Huo, X. Sun, T. Ikegami, and T. Ishigaki <i>J. Am. Ceram. Soc.</i> , Vol. 91, No. 2, p. 603-606, 2008	49
A Pulse Combustion-Spray Pyrolysis Process for the Preparation of Nano- and Submicrometer-Sized Oxide Particles W. Widiyastuti, Wei-Ning Wang, Agus Purwanto, I. Wuled Lenggoro, and Kikuo Okuyama <i>J. Am. Ceram. Soc.</i> , Vol. 90, No. 12, p. 3779-3785, 2007	53
One-Step Synthesis of Luminescent Nanoparticles of Complex Oxide, Strontium Aluminate C. Li, Y. Imai, Y. Adachi, H. Yamada, K. Nishikubo, and C-N Xu <i>J. Am. Ceram. Soc.</i> , Vol. 90, No. 7, p. 2273-2275, 2007	61
Nano α - Al_2O_3 Powder Preparation by Calcining an Emulsion Precursor Y-C Lee, S-B Wen, L. Wenglin, and C-P Lin <i>J. Am. Ceram. Soc.</i> , Vol. 90, No. 6, p. 1723-1727, 2007	65

Lanthanum Strontium Manganite Powders Synthesized by Gel-Casting for Solid Oxide Fuel Cell Cathode Materials	71
L. Zhang, Y. Zhang, Y. Zhen, and S. Jiang <i>J. Am. Ceram. Soc.</i> , Vol. 90, No. 5, p. 1406-1411, 2007	
Preparation of Matrix-Type Nickel Oxide/Samarium-Doped Ceria Composite Particles by Spray Pyrolysis	77
S. Suda, K. Kawahara, M. Kawano, H. Yoshida, and T. Inagaki <i>J. Am. Ceram. Soc.</i> , Vol. 90, No. 4, p. 1094-1100, 2007	
Novel Low-Temperature Synthesis of Ferroelectric Neodymium-Doped Bismuth Titanate Nanoparticles	85
P. Prakash, A. Garg, M. Roy, and H. Verma <i>J. Am. Ceram. Soc.</i> , Vol. 90, No. 4, p. 1295-1298, 2007	
Hydrothermal Synthesis of CdMoO ₄ Nano-Particles	89
X. Jiang, J. Ma, B. Lin, Y. Ren, J. Liu, X. Zhu, J. Tao, Y. Wang, and L. Xie <i>J. Am. Ceram. Soc.</i> , Vol. 90, No. 3, p. 977-979, 2007	
Chromium-Doped Forsterite Nanoparticle Synthesis by Flame Spray Pyrolysis	93
T. Tani, S. Saeki, T. Susuki, and Y. Ohishi <i>J. Am. Ceram. Soc.</i> , Vol. 90, No. 3, p. 805-808, 2007	
Formation of Al ₂ O ₃ -TiC Composite Nano-Particles Synthesized from Carbon-Coated Precursors	97
H. Kaga and R. Koc <i>J. Am. Ceram. Soc.</i> , Vol. 90, No. 2, p. 407-411, 2007	
Synthesis of Sm _{0.5} Sr _{0.5} CoO _{3-x} and La _{0.6} Sr _{0.4} CoO _{3-x} Nanopowders by Solution Combustion Process	103
N. Bansal and Z. Zhong <i>CT</i> , Vol. 195, p. 23-32, 2006	
Colloidal Processing and Sintering of Nano-ZrO ₂ Powders Using Polyethylenimine	113
Y. Hotta, C. Duran, K. Sato, and K. Watari <i>CT</i> , Vol. 190, p. 85-93, 2006	
Synthesis of High Purity β-SiAlON Nanopowder from a Zeolite by Gas-Reduction-Nitridation	123
T. Yamakawaa, T. Wakiyara, J. Tatami, K. Komeya, and T. Meguro <i>CT</i> Vol. 190, p. 3-8, 2006	
A Novel Supercritical CO ₂ Synthesis of Amorphous Hydrous Zirconia Nanoparticles, and Their Calcination to Zirconia	129
M-H Lee, H-Y Lin, and J. L. Thomas <i>J. Am. Ceram. Soc.</i> , Vol. 89, No. 12, p. 3624-3630, 2006	
Praseodymium-Doped Photo-Luminescent Strontium Indate Nanoparticles by Ultrasonic Spray Pyrolysis	137
S. E. Lin, K. Borgohain, and W. C. J. Wei <i>J. Am. Ceram. Soc.</i> , Vol. 89, No. 10, p. 3266-3269, 2006	
Nano-Blast Synthesis of Nano-size CeO ₂ -Gd ₂ O ₃ Powders	141
Oleg Vasylykiv, Yoshio Sakka and Valeriy V. Skorokhod <i>J. Am. Ceram. Soc.</i> , Vol. 89, No. 6, p. 1822-1826, 2006	
Sol-Gel Processing and Characterization of Phase-Pure Lead Zirconate Titanate Nano-Powders	147
Yasir Faheem and M. Shoaib <i>J. Am. Ceram. Soc.</i> , Vol. 89, No. 6, p. 2034-2037, 2006	
Synthesis of AlN Nanopowder from γ-Al ₂ O ₃ by Reduction-Nitridation in a Mixture of NH ₃ -C ₃ H ₈	151
Tomohiro Yamakawa, Junichi Tatami, Toru Wakiyara, Katsutoshi Komeya, Takeshi Meguro, Kenneth J. D. MacKenzie, Shinichi Takagi, and Masahiro Yokouchi <i>J. Am. Ceram. Soc.</i> , Vol. 89, No. 1, p. 171-175, 2006	

Membranes, Films, and Coatings

Microporous ZrO ₂ Membrane Preparation by Liquid-Injection MOCVD	159
S. Mathur, E. Hemmer, S. Barth, J. Altmayer, N. Donia, I. Kumakiri, N. Lecerf, and R. Bredesen <i>CESP</i> , Vol. 28, No. 6, p. 165-173, 2008	

Growth of Barium Hexaferrite Nanoparticle Coatings by Laser-Assisted Spray Pyrolysis G. Dedigamuwa, P. Mukherjee, H. Srikanth, and S. Witanachchi <i>CESP</i> , Vol. 28, No. 6, p. 73-81, 2008	169
Two Phase Monazite/Xenotime $30\text{LaPO}_4\text{-}70\text{YPO}_4$ Coating of Ceramic Fiber Tows E. Boakye, R. Hay, P. Mogilevsky, and M. Cinibulk <i>J. Am. Ceram. Soc.</i> , Vol. 91, No. 1, p. 17-25, 2008	179
Template-Free Self-Assembly of a Nanoporous TiO_2 Thin Film Y. Gao, M. Nagai, W-S Seo, and K. Koumoto <i>J. Am. Ceram. Soc.</i> , Vol. 90, No. 3, p. 831-837, 2007	189
Nano-Sized Hydroxyapatite Coatings on Ti Substrate with TiO_2 Buffer Layer by E-beam Deposition S-H Lee, H-E Kim, and H-W Kim <i>J. Am. Ceram. Soc.</i> , Vol. 90, No. 1, p. 50-56, 2007	197
Sol-Gel Routes to Nanostructured Patterned Ferroelectric Thin Films with Novel Electronic and Optical Functions M. Kuwabara, Y. J. Wu, J. Li, and T. Koga <i>Ceramic Transactions</i> , Vol. 196, p. 371-380, 2006	205
Preparation and Properties of Hydrothermally Stable γ -Alumina-Based Composite Mesoporous Membranes Md. Hasan Zahir, Koji Sato, Hiroshi Mori, Yuji Iwamoto, Mikihiro Nomura, and Shin-ichi Nakao <i>J. Am. Ceram. Soc.</i> , Vol. 89, No. 9, p. 2874-2880, 2006	215
Synthesis and Tribological Behavior of Silicon Oxycarbonitride Thin Films Derived from Poly(Urea)Methyl Vinyl Silazane T. Cross, R. Raj, T. Cross, S. Prasad, and D. Tallant <i>Int. J. of Appl. Ceram. Technol.</i> , Vol. 3 No. 2, p. 113-126, 2006	223
Synthesis and Tribology of Carbide-Derived Carbon Films A. Erdemir, A. Kovalchenko, C. White, R. Zhu, A. Lee, M. J. McNallan, B. Carroll and Y. Gogotsi <i>Int. J. of Appl. Ceram. Technol.</i> , Vol. 3, No. 3, p. 236-244, 2006	237
Nanotubes, Nanorods, and Nanowires	
Design, Fabrication and Electronic Structure of Oriented Metal Oxide Nanorod-Arrays L. Vayssieres <i>CESP</i> , Vol. 28, No. 6, p. 187-193, 2008	249
Electrospinning of Alumina Nanofibers K. Lindqvist, E. Carlström, A. Nelvig, and B. Hagström <i>CESP</i> , Vol. 28, No. 6, p. 41-51, 2008	257
ZnO Nanofiber and Nanoparticle Synthesized Through Electrospinning and Their Photocatalytic Activity Under Visible Light H. Liu, J. Yang, J. Liang, Y. Huang, and C. Tang <i>J. Am. Ceram. Soc.</i> , Vol. 91, No. 4, p. 1287-1291, 2008	269
Synthesis of Carbon Nanotubes and Silicon Carbide Nanofibers as Composite Reinforcing Materials H. Li, A. Kothari, and B. W. Sheldon <i>CESP</i> , Vol. 27, No. 8, p. 41-48, 2007	275
Polymer Fiber Assisted Processing of Ceramic Oxide Nano and Submicron Fibers S. Shukla, E. Brinley, H. J. Cho, and S. Seal, <i>CESP</i> , Vol. 27, No. 8, p. 57-68, 2007	283
Growth of Quasi-Aligned AlN Nanofibers by Nitriding Combustion Synthesis M. Radwan and Y. Miyamoto <i>J. Am. Ceram. Soc.</i> , Vol. 90, No. 8, p. 2347-2351, 2007	295

Synthesis and Optical Properties of Mullite Nanowires H-K Seong, U. Kim, M-H Kim, H-J Choi, Y. Lee, and W-S Seo <i>J. Am. Ceram. Soc.</i> , Vol. 90, No. 6, p. 1937-1939, 2007	301
(Na _{0.8} K _{0.2}) _{0.5} Bi _{0.5} TiO ₃ Nanowires: Low-Temperature Sol-Gel-Hydrothermal Synthesis and Densification Y-D Hou, L. Hou, T-T Zhang, M-K Zhu, H. Wang, and H. Yan <i>J. Am. Ceram. Soc.</i> , Vol. 90, No. 6, p. 1738-1743, 2007	305
Synthesis and Characterization of Ce _{1-x} Gd _x O _{2-δ} Nanorods J. S. Lee and S. Kim <i>J. Am. Ceram. Soc.</i> , Vol. 90, No. 2, p. 661-663, 2007	311
Synthesis and Characterization of Cubic Silicon Carbide (β-SiC) and Trigonal Silicon Nitride (α-Si ₃ N ₄) Nanowires K. Saulig-Wenger, M. Bechelany, D. Cornu, S. Bernard, F. Chassagneux, P. Miele, and T. Epiciers <i>CESP</i> , Vol. 27, No. 8, p. 81-88, 2007	315
Synthesis of Boron Nitride Nanotubes for Engineering Applications J. Hurst, D. Hull, and D. Gorican <i>CESP</i> , Vol. 27, No. 8, p. 95-102, 2007	323
Novel Process of Submicron-Scale Ceramic Rod Array Formation on Metallic Substrate K. Okamoto, S. Hayakawa, K. Tsuru, and A. Osaka <i>CT</i> , Vol. 195, p. 133-138, 2006	331
Tin Oxide Nanoparticle-Functionalized Multi-Walled Carbon Nanotubes by the Vapor Phase Method W. Fan, L. Gao, and J. Sun <i>J. Am. Ceram. Soc.</i> , Vol. 89, No. 8, p. 2671-2673, 2006	337
Electrospinning: A Simple and Versatile Technique for Producing Ceramic Nanofibers and Nanotubes D. Li, J. McCann, Y. Xia, and M. Marquez <i>J. Am. Ceram. Soc.</i> , Vol. 89, No. 6, p. 1861-1869, 2006	341
Nanocomposites and Nanostructures	
Chemical Precipitation Synthesis and Optical Properties of ZnO/SiO ₂ Nanocomposites H. Yang, Y. Xiao, K. Liu, and Q. Feng <i>J. Am. Ceram. Soc.</i> , Vol. 91, No. 5, p. 1591-1596, 2008	353
Low-Temperature Processing of Dense Hydroxyapatite-Zirconia Composites Y. Nayak, R. Rana, S. Pratihari, and S. Bhattacharyya <i>Int. J. Appl. Ceram. Technol.</i> , Vol. 5, No. 1, p. 29-36, 2008	359
Synthesis and Characterization of Chalcogenide Nanocomposites J. Martin and G. Nolas <i>CESP</i> , Vol. 28, No. 8, p. 221-226, 2008	367
Self Assembled Functional Nanostructures and Devices C. S. Ozkan <i>CESP</i> , Vol. 28, No. 6, p. 91-94, 2008	373
Carbon Nanotube (CNT) and Carbon Fiber Reinforced High Toughness Reaction Bonded Composites P. Karandikar, G. Evans, and M. Aghajanian <i>CESP</i> , Vol. 28, No. 6, 2008, p. 53-63, 2007	377
Synthesis, Characterization and Measurements of Electrical Properties of Alumina-Titania Nanocomposites V. Somani and S. Kalita <i>CESP</i> , Vol. 27, No. 8, p. 11-22, 2007	389
A New Ternary Nanolaminate Carbide: Ti ₃ SnC ₂ S. Dubois, T. Cabioc'h, P. Chartier, V. Gauthier, and M. Jaouen <i>J. Am. Ceram. Soc.</i> , Vol. 90, No. 8, p. 2642-2644, 2007	401

Fabrication of a Nano-Si ₃ N ₄ /Nano-C Composite by High-Energy Ball Milling and Spark Plasma Sintering X. Xu, T. Nishimura, N. Hirotsaki, R-J Xie, and H. Tanaka <i>J. Am. Ceram. Soc.</i> , Vol. 90, No. 4, p. 1058-1062, 2007	405
Conversion of Bamboo to Biomorphic Composites Containing Silica and Silicon Carbide Nanowires T. L. Y. Cheung and D. H. L. Ng <i>J. Am. Ceram. Soc.</i> , Vol. 90, No. 2, p. 559-564, 2007	411
Novel Processing to Produce Polymer/Ceramic Nanocomposites by Atomic Layer Deposition X. Liang, L. Hakim, G-D Zhan, J. McCormick, S. George, A. Weimer, J. Spencer II, K. Buechler, J. Blackson, C. Wood, and J. Dorgan <i>J. Am. Ceram. Soc.</i> , Vol. 90, No. 1, p. 57-63, 2007	417
Intra-Type Nanocomposites for Strengthened and Toughened Ceramic Materials S. Choi, S. Honda, S. Hashimoto, and H. Awaji <i>CT</i> , Vol. 190, p. 173-180, 2006	425
Preparation and Properties of Mullite-Based Iron Multi-Functional Nanocomposites H. Wang, W. Wang, Z. Fu, T. Sekino, and K. Niihara <i>CT</i> , Vol. 190, p. 203-211, 2006	433
Electrospinning of Ceramic Nanofibers and Nanofiber Composites J. Yuh, H. Park, and W. Sigmund <i>Ceramic Transactions</i> , Vol. 190, p. 9-19, 2006	443
Microstructure and Properties of Spark Plasma-Sintered ZrO ₂ -ZrB ₂ Nanoceramic Composites B. Basu, T. Venkateswaran, and D-Y Kim <i>J. Am. Ceram. Soc.</i> , Vol. 89, No. 8, p. 2405-2412, 2006	455
Homogeneous ZrO ₂ -Al ₂ O ₃ Composite Prepared by Nano-ZrO ₂ Particle Multilayer-Coated Al ₂ O ₃ Particles Y. Jia, Y. Hotta, K. Sato, and K. Watari <i>J. Am. Ceram. Soc.</i> , Vol. 89, No. 3, p. 1103-1106, 2006	463
Preparation of a Highly Conductive Al ₂ O ₃ /TiN Interlayer Nanocomposite through Selective Matrix Grain Growth X. Jin and L. Gao <i>J. Am. Ceram. Soc.</i> , Vol. 89, No. 3, p. 1129-1132, 2006	467
Preparation and Microstructure of Multi-Wall Carbon Nanotubes-Toughened Al ₂ O ₃ Composite J. Fan, D. Zhao, M. Wu, Z. Xu, and J. Song <i>J. Am. Ceram. Soc.</i> , Vol. 89, No. 2, p. 750-753, 2006	471
Three-Dimensional Assemblies of Zirconia Nanocrystals Via Shape-Preserving Reactive Conversion of Diatom Microshells S. Shian, Y. Cai, M. Weatherspoon, S. Allan, and K. Sandhage <i>J. Am. Ceram. Soc.</i> , Vol. 89, No. 2, p. 694-698, 2006	475

Synthesis Methods for Powders

Freeze Casting as a Nanoparticle Material-Forming Method

Kathy Lu^{*,†} and Xiaojing Zhu^{*}

Materials Science and Engineering Department, Virginia Polytechnic Institute and State University, Blacksburg, Virginia 24061

Nanoparticle material forming is challenging because of loose packing and agglomeration issues intrinsic to nanoparticles. Liquid processing shows great potential to overcome such hurdles. This study is focused on nanoparticle colloidal processing and freeze-casting forming. Al_2O_3 nanoparticle suspensions are examined, and microstructure evolution of Al_2O_3 nanoparticle suspension during freeze casting is discussed. The “Fines” effect influences nanoparticle packing on freeze-cast sample surfaces. Trapped air bubbles in the suspension lead to a porous bulk microstructure. Prerest is necessary for dense and homogeneous green microstructure formation. The green strength, fracture mode, and ability to form fine features by freeze casting are also evaluated.

Introduction

The huge surface area intrinsic to nanoparticles serves as one of the most striking advantages as well as disadvantages for nanoparticle material forming. Because of the natural tendency of nanoparticles in forming agglomerates, wet forming utilizing a colloidal suspension has become the most active research area in nanoceramics. For almost all the nanoparticle wet forming processes, the first step is to produce a stable colloidal suspension. A green body with a uniform

microstructure can then be produced from the fully stabilized colloidal suspension of nanoparticles.

Freeze casting is a process that pours the suspension into a nonporous mold, freezes the suspension, demolds the frozen sample, and then dries the sample under vacuum. Liquid-state to solid-state conversion is realized through phase transformation of the dispersing medium such as water. The process has the potential to form near net-shape complex geometry parts with low pressure and often environmentally benign advantages.^{1,2} The key requirements are that the suspension is stable and unagglomerated.³ When the freeze-casting condition is properly controlled, water separates from solid phases through sublimation and no capillary force exists to cause hard agglomerates or cracks.⁴

Freeze casting has been practiced for some time.^{1,2,5,6} However, the studies were mainly focused on micrometer-sized particles and large-sized samples. For example, Al_2O_3 particles of 0.4 μm were freeze cast

Supported by Petroleum Research Fund, administered through American Chemical Society.

Presented at the 31st International Conference on Advanced Ceramics and Composites, Daytona Beach, FL, January 21–26, 2007.

^{*}Member, The American Ceramic Society.

[†]klu@vt.edu

© 2008 The American Ceramic Society

and >98% sintered density was achieved.⁷ Enclosed shells of Al₂O₃ bodies encapsulating steel parts were fabricated.⁸ Porous and layered-hybrid materials were freeze cast.⁹ However, application of freeze casting to nanoparticle systems and understanding the freeze-casting behaviors of nanoparticle suspensions have not been explored. One challenge is that nanoparticle research in forming bulk components is still evolving; considerable effort is still needed in achieving high solids loading suspensions. The other challenge is the drastic capillary pressure increase with decreasing particle size; it takes a prolonged duration of time and much improved control to remove water completely by sublimation. Our past work has addressed the first challenge to a certain extent.^{10–12} To address the second challenge successfully, it is essential to understand the nanoparticle microstructure evolution from the colloidal state to the freeze-dried state.

High particle packing efficiency is preferred for postfreeze casting, handling, and densification purposes. Freeze-cast sample strength and failure mode can be used to understand and evaluate this aspect. With the decrease of particle size to nanoscale, the feature sizes of nanoparticle samples can also be correspondingly decreased. The potential in forming fine features by freeze casting should be explored.

This study is focused on Al₂O₃ nanoparticle suspension viscosity evaluation and the corresponding freeze casting process for solid sample formation. Microstructural evolution of nanoparticle suspensions from a colloidal state to a freeze-dried state is examined. The surface and bulk microstructures under different pretest conditions are compared. Special nanoparticle phenomena during the suspension to solid-state transformation are explained. Equibiaxial strength and fracture mode of the freeze-cast samples are examined. Fine features produced by the freeze-casting process are presented.

Experimental Procedure

Al₂O₃ dry nanoparticles with a specific surface area of 45 m²/g were used in this study (Nanophase Technologies, Romeoville, IL). The particles can be redispersed in water by ball milling as reported before by transmission electron microscopy (TEM) analysis.¹⁰ In this study, the particle size distribution was further measured by a dynamic light-scattering measurement

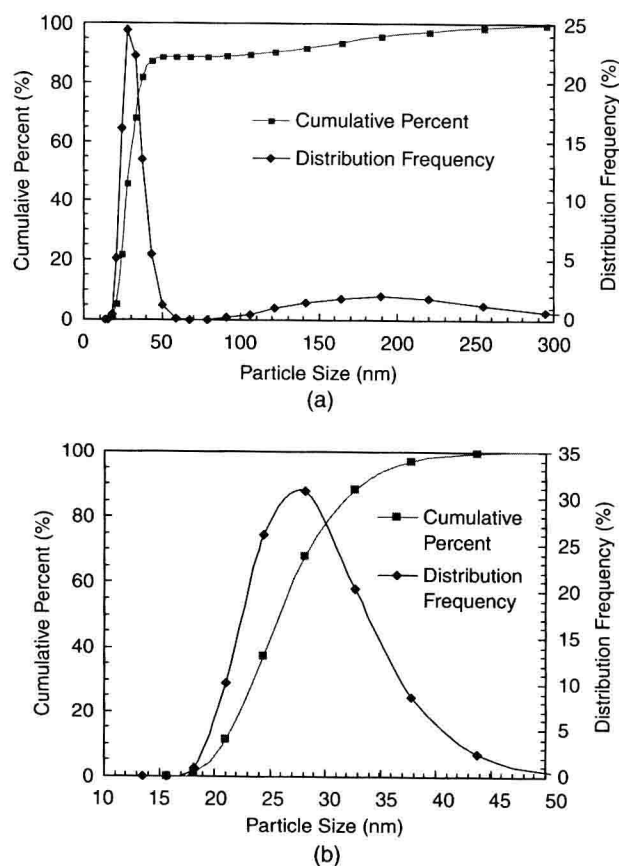


Fig. 1. Al₂O₃ nanoparticle size distribution from dynamic light scattering analysis: (a) weight basis, (b) number basis.

as shown in Fig. 1 (Zetasizer Nano ZS, Malvern Instruments Inc., Southborough, MA). Agglomerates are absent. However, Al₂O₃ nanoparticles are polydispersed, consistent with the TEM analysis. Even though on the weight basis there seems to be ~10 wt% of >100 nm particles, on the number basis, large particles are negligible (<0.5%). For the Al₂O₃ nanoparticle suspension preparation, poly(acrylic acid) (PAA, M_w 1800, Aldrich, St. Louis, MO) was used as the dispersant with the segment as $[-CH_2CH(CO_2H)-]$ and glycerol (C₃H₈O₃, Fisher Chemicals, Fairlawn, NJ) was used as the freeze casting aid with the molecular formula CH₂OH-CHOH-CH₂OH. A water-glycerol mixture at a weight ratio of 10:1 (water:glycerol) was used as the dispersing medium. The mixture was homogenized for 5 min using a ball mill (755 RMV, US Stoneware, East Palestine, OH) before use, and the ball mill rotation speed was 75 rpm. Al₂O₃ nanoparticles were added to the dispersing medium in 10 g increments along with a PAA dispersant at 2.0 wt% of Al₂O₃. Because low pH

promotes PAA dispersant adsorption onto Al_2O_3 nanoparticles,¹³ HCl solution was added to lower the pH to 1.5. The suspension was ball milled for 12 h with periodic adjustment of pH to 1.5. The purpose of the ball milling was to break the soft agglomerates of the dry Al_2O_3 nanoparticles and thoroughly homogenize water, glycerol, PAA, and Al_2O_3 nanoparticles. The milling media were Al_2O_3 rods with 6 mm diameter and 6 mm height. Breaking down of Al_2O_3 nanoparticles into smaller sizes was believed to be absent because of the low energy that ball milling provided. However, air bubbles can be introduced into the suspension during mixing. Suspensions of approximately 20 vol% Al_2O_3 solids loading were made by this procedure. After this step, Al_2O_3 nanoparticles were again added in 10 g increments, along with a PAA dispersant at 2.0 wt% of Al_2O_3 in order to make a 40 vol% solids loading suspension. The final PAA amount was thus maintained at 2.0 wt% of Al_2O_3 . NH_4OH (28–30 wt%, VWR International, West Chester, PA) was used to adjust the suspension to pH 9.5 in order to achieve the highest suspension flowability for freeze casting.¹⁰ It should be pointed out that the liquid volume of NH_4OH and HCl was considered for the 40 vol% solids loading reported. The suspension was then mixed for 24 h for complete homogenization.

Suspension viscosities without and with glycerol were characterized using a rheometer with a cone-plate geometry (AR 2000, TA Instruments, New Castle, DE). All the viscosity measurements were performed with a controlled shear rate in a decreasing shear rate order. Freeze-casting molds were developed using poly(dimethylsiloxane) epoxy (RTV 664, General Electric Company, Waterford, NY). An Al_2O_3 suspension was filled into the mold immediately after the suspension preparation. Some of the filled molds were kept under ambient conditions for 1 h; other filled molds were frozen in a freeze dryer (Labconco Stoppering Tray Dryer, Labconco, Kansas City, MO) immediately. This 1-h resting period after the mold filling but before the freeze-casting step is termed as prerest in the following discussion. During the freezing process, the suspension-filled molds were kept at -35°C for 2 h. Then, the samples were demolded and exposed to vacuum ($<1 \times 10^4$ Pa) to allow ice to sublime for 36 h. The microstructural differences in the freeze-cast samples with and without prerest were systematically analyzed using a LEO550 field emission scanning electron microscope (SEM) (Carl Zeiss MicroImaging Inc., Thornwood, NY).

For the freeze-dried sample green strength measurement, circular disks 25.4 mm in diameter and 1.58 mm in thickness were freeze cast. The Al_2O_3 suspension was placed in the mold cavity using a disposable pipette. Care was taken to fill the molds completely with the Al_2O_3 suspension. After the mold filling, the samples were allowed to rest for 1 h under ambient conditions. The fracture load was measured using a Texture Analyzer test console (Stable Micro Systems, Surrey, U.K.), equipped with a 5 kN load cell. The equibiaxial flexural strength was then calculated for each sample, using the following equation:

$$\sigma_f = \frac{3F}{2\pi b^2} \left[\frac{(1-\nu)D_s^2 - D_L^2}{2D^2} + (1+\nu) \ln \frac{D_s}{D_L} \right] \quad (1)$$

where σ_f is the fracture strength in units of MPa, F is the fracture load in units of N, b is the specimen thickness in units of mm, ν is Poisson's ratio, D is the sample diameter in mm, D_s is the diameter of the support ring in mm, and D_L is the diameter of the load ring in mm.

Results and Discussion

Al_2O_3 Nanoparticle Suspensions

In the previous study,¹¹ it was identified that for the Al_2O_3 nanoparticle suspension studied, the PAA amount adsorbed onto Al_2O_3 particles increases with PAA concentration increase up to 2.00 wt% of Al_2O_3 . As more PAA is added to the suspension, the PAA amount adsorbed reaches a plateau of 0.31 mg/m². The adsorption plateau represents the adsorption saturation at which the Al_2O_3 particle surfaces are fully covered by the PAA dispersant. Also, the suspension has the lowest viscosity from pH 7.5 to 9.5; this pH range is the most desirable pH range for stabilizing the Al_2O_3 nanoparticles. Based on these results, the PAA concentration is 2.00 wt% of Al_2O_3 and the pH is 9.5 for the Al_2O_3 nanoparticle suspensions in this study.

Figure 2 shows the viscosities for the 20–45 vol% Al_2O_3 solids loading suspensions. The viscosities are a strong function of Al_2O_3 nanoparticle solids loading. With an increase in Al_2O_3 solids loading, the viscosity increases at all shear rates. Approximately, the suspension viscosity increases by two orders of magnitude from 20 to 45 vol% solids loading. As the shear rate increases,

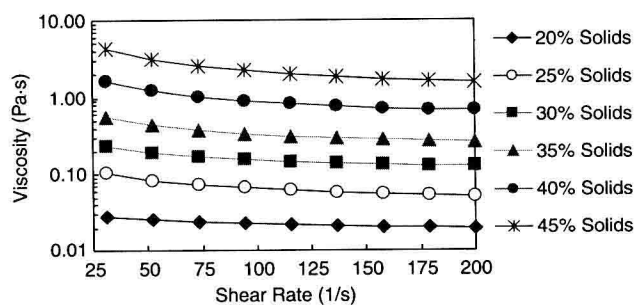


Fig. 2. Viscosity change versus shear rate for different Al_2O_3 solids loading suspensions. Each curve is an average of three measurements and the standard deviation is much smaller than the markers and cannot be shown on the figure.

the viscosity decreases monotonically but the Al_2O_3 nanoparticle suspension does not obey Newtonian flow. Instead, the suspension displays a shear-thinning behavior, reflecting the broken polymeric link between the nanoparticles provided by the PAA dispersant. At 20 vol% solids loading, the viscosity changes from 0.03 to 0.02 Pa.s when the shear rate is changed from 30 to 200 s^{-1} . At 45 vol% solids loading, the viscosity changes from 4.35 to 1.60 Pa.s when the shear rate is changed from 30 to 200 s^{-1} . As the Al_2O_3 solids loading increases, the viscosity difference becomes much larger at high solids loading levels. This indicates that the suspension undergoes a more drastic “link breakage” and that the suspension conditions should be controlled more rigorously and optimized under high solids loading conditions.

There are two states for a polydispersed nanoparticle suspension like the Al_2O_3 suspension studied here: fluid and glass, depending on solids loading.¹⁴ For freeze casting, especially when forming parts with complex shapes, the suspension should be kept at reasonably high solids loading levels. When the solids loading is too low, the freeze-cast sample will have a very low particle packing density and present a challenge for densification. However, when the solids loading is too high, the suspension will be too viscous to flow into the fine features of the mold. Ideally, the solids loading should be chosen at the boundary of fluid and glass suspensions, slightly on the fluid-state side. Our prior study has identified that 45% solids loading is approximately near the fluid-state to glass-state boundary region.¹⁵ Based on this consideration, the suspension of 40 vol% Al_2O_3 solids loading was used for the freeze-casting studies reported here.

Prerest Effect

In the previous work,¹¹ the critical role of prerest in forming homogenous and crack-free freeze-cast samples was reported. However, the microstructural changes were not understood. In this study, the prerest effects on the freeze-cast sample microstructure evolution are examined from two aspects: surface microstructure and bulk microstructure.

The free surface microstructures of the freeze-cast samples without and with prerest are shown in Fig. 3. For the sample without prerest (Fig. 3a), the surface is rather flat and the Al_2O_3 particles are densely packed. For the sample with prerest (Fig. 3b), the surface is rough and the particles are loosely packed. This surface smoothness difference can be observed indirectly from

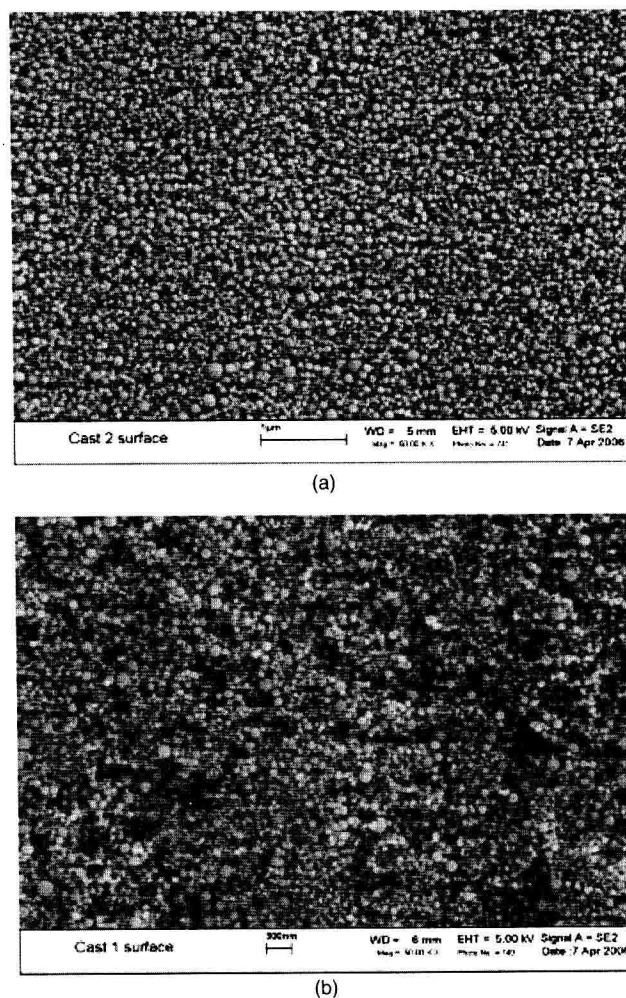


Fig. 3. Surface microstructure difference for the freeze-cast samples: (a) without prerest, (b) with prerest.

the surface luster difference. For the sample in Fig. 3a, the surface is shiny. For the sample in Fig. 3b, the surface is dull. The unique nature of the freeze casting process is able to capture this evolution that otherwise would be missed unless *in situ* analysis is used.¹⁶

Figure 3 reveals phenomena that are in sharp contrast with the well-established understanding at the micrometer particle size level. Even though the gravity effect seems to be a convenient explanation, it can be eliminated because the suspension is stabilized to prevent sedimentation and the particle size is too small for gravity to play an essential role within the timeframe studied. Lue and Woodcock¹⁷ generalized this particle self-arrangement process as the “fines” effect and showed that the large to small particle size ratio for the “fines” effect to be effective is 10:1. The “fines” effect refers to the natural tendency of the small particles migrating to fill the space between the large particles under Brownian motion when the suspension is kept undisturbed. From Fig. 1, the Al_2O_3 nanoparticle suspension certainly meets this particle size criterion. During the undisturbed prerest time period, Brownian motion causes nanoparticles to move within the suspension. When the small nanoparticles migrate to fill the voids between the large nanoparticles, the process causes the large particles on the suspension surface to open up the network to accommodate the highly diffusive small particles. The net result is a more open and less smooth surface microstructure. This observation clearly indicates that Brownian motion is an important phenomenon affecting nanoparticle material surface microstructures. From the freeze-cast surface microstructure comparison, it can be concluded that nanoparticle size distribution plays an important role when the suspension is directly frozen, even if the large particles only take up a small percent of the overall distribution. The particle size distribution should be kept at the narrowest range for suspension-related forming processes if a uniform and consistent surface microstructure is desired.

The fracture surface microstructures of the freeze-cast Al_2O_3 samples are shown in Fig. 4. Figure 4a shows the sample without prerest. Figure 4b shows the sample with prerest. Both samples are formed under the same freeze-casting conditions. For the sample without prerest (Fig. 4a), a porous bulk microstructure develops and the pores are $\sim 3\ \mu\text{m}$ in size through SEM image measurement of about 50 pores. For the sample with prerest, no micrometer-sized pores are present as shown in Fig. 4b. For the Al_2O_3 nanoparticle suspension preparation,

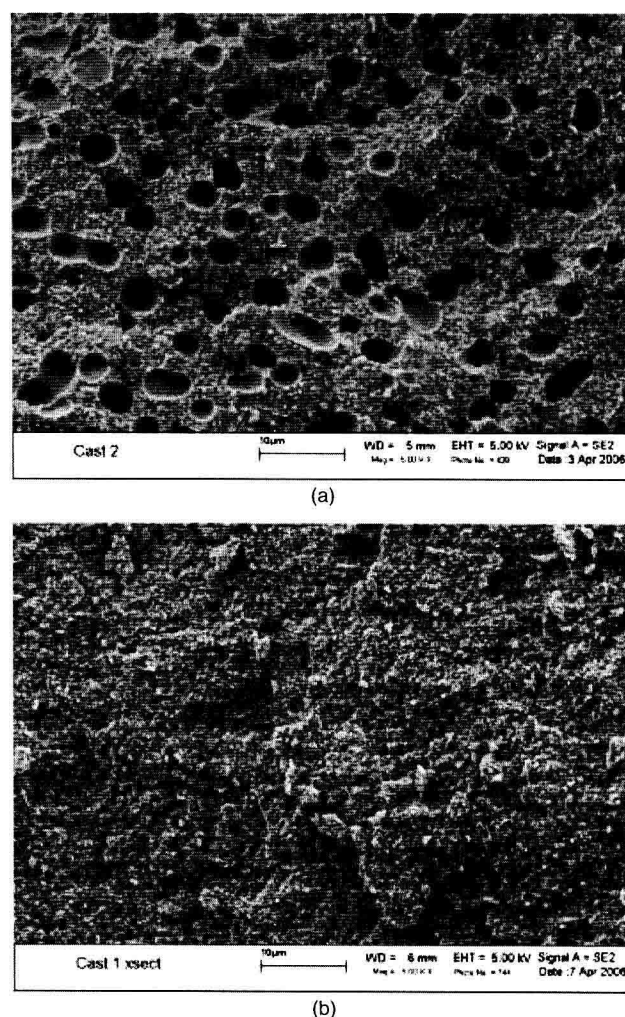


Fig. 4. Bulk microstructure difference for the freeze-cast samples: (a) without prerest, (b) with prerest.

a high shear process, ball milling, was used to homogenize Al_2O_3 nanoparticles, dispersant PAA, glycerol, and water. A shear force was constantly present to break the nanoparticle suspension and encapsulate air bubbles while homogenizing the suspension. When the shear ceases, the Al_2O_3 nanoparticle suspension should be given time to reorganize for the air bubbles to migrate out of the suspension. However, it may take a long time to eliminate the air bubbles completely for the high solids loading suspensions due to the relatively higher suspension viscosity and more particle movement hindrance. If the nanoparticle suspension is frozen before such an equilibrium is reached, then observations are often made for a metastable suspension with air bubbles dispersed in the suspension.